INTERNATIONAL JOURNAL FOR NUMERICAL METHODS IN ENGINEERING
Int. J. Numer. Meth. Engng 2000; **48**:351–373

Design sensitivity analysis and optimization of non-linear transient dynamics. Part I—sizing design

Seonho Cho and K. K. Choi*,†

Center for Computer-Aided Design and Department of Mechanical Engineering, College of Engineering, The University of Iowa, Iowa City, IA 52242, U.S.A.

SUMMARY

A continuum-based sizing design sensitivity analysis (DSA) method is presented for the transient dynamic response of non-linear structural systems with elastic–plastic material and large deformation. The methodology is aimed for applications in non-linear dynamic problems, such as crashworthiness design. The first-order variations of the energy forms, load form, and kinematic and structural responses with respect to sizing design variables are derived. To obtain design sensitivities, the direct differentiation method and updated Lagrangian formulation are used since they are more appropriate for the path-dependent problems than the adjoint variable method and the total Lagrangian formulation, respectively. The central difference method and the finite element method are used to discretize the temporal and spatial domains, respectively. The Hughes–Liu truss/beam element, Jaumann rate of Cauchy stress, rate of deformation tensor, and Jaumann rate-based incrementally objective stress integration scheme are used to handle the finite strain and rotation. An elastic–plastic material model with combined isotropic/kinematic hardening rule is employed. A key development is to use the radial return algorithm along with the secant iteration method to enforce the consistency condition that prevents the discontinuity of stress sensitivities at the yield point. Numerical results of sizing DSA using DYNA3D yield very good agreement with the finite difference results. Design optimization is carried out using the design sensitivity information. Copyright © 2000 John Wiley & Sons, Ltd.

KEY WORDS: sizing design sensitivity; transient dynamics; elastic–plastic material; finite strain and rotation; DYNA3D

1. INTRODUCTION

There have been a limited number of research results in DSA of transient dynamic response of non-linear structural systems with elastic–plastic material and large deformation. Choi and Santos [1, 2] presented a unified approach for sizing DSA of non-linear structural systems that included truss, beam, plane elastic solid and plate components. Park and Choi [3] developed

*Correspondence to: K. K. Choi, Department of Mechanical Engineering, Center for Computer-Aided Design, The University of Iowa, Iowa City, IA 52242, U.S.A.
†E-mail: kkchoi@ccad.niowa.edu

Contract/grant sponsor: U.S. Army TARDEC

Received 20 October 1998
Revised 30 June 1999

a continuum DSA method for responses of non-linear structural systems with rate-independent elastic–plastic material under small deformation and small strain assumptions for truss and membrane elements. Lee and Arora [4] developed a sizing DSA method for structural systems with elastic–plastic material using the continuum formulation and implemented using their in-house FEA code. Tsay and Arora [5] applied the non-linear DSA method to path-dependent problems with small strain assumption using the total Lagrangian formulation. Vidal and Haber [6] used an implicit integration scheme and the consistent tangent operator for DSA of structures with elastic–plastic materials. The consistent tangent stiffness matrix obtained at the end of the constitutive iteration of FEA was used to update the response sensitivities at the current time step. With the consistency between equilibrium and constitutive iterations, no iterations were required to evaluate the constitutive relation in the design sensitivity formulation.

Hughes and Liu [7, 8] presented a non-linear finite element formulation to account for finite strain and rotation effects. They presented a non-linear constitutive algorithm, which is incrementally objective for large rotational increments and maintains the zero normal stress condition in the rotating stress co-ordinate system. Hughes *et al.* [9, 10] discussed the construction of the element and the lumped mass matrices and showed that the critical time steps for transient analysis can be larger if the lumped mass matrix is used. An elastic–plastic material model that is time-independent, non-thermal, isotropic, and combined isotropic/kinematic hardening rule with the von Mises yield surface and associative flow rule was proposed by Krieg and Key [11].

Even with these advancements, there is still a lack of effective methods that are applicable to optimum design of structural non-linear dynamic problems such as crashworthiness. In this paper, the update Lagrangian formulation and direct differentiation method, that are more appropriate for the path-dependent problems than the total Lagrangian formulation and adjoint variable method, are applied to derive the design sensitivity formulations. The sensitivity information is used for design optimization of a vehicle frame.

2. NON-LINEAR TRANSIENT DYNAMIC ANALYSIS

The left subscript and left superscript denote the reference and the designated configuration numbers, respectively. The right subscript and superscript represent the tensor component and the iteration counter, respectively. Unless the configuration number is specified, the current configuration $(n+1)$ is assumed. The following are used to simplify notations:

$\Delta(\bullet) \equiv {}^{n+1}_{n}(\bullet)$: incremental quantity,
$(\bullet) \equiv {}^{n+1}(\bullet)$: total quantity at the current configuration $(n+1)$,
$\Gamma \equiv {}^{n}\Gamma$, $\Omega \equiv {}^{n}\Omega$: boundary and domain at the previous configuration (n), respectively.

The equations of motion (Cauchy's first law of motion) of an arbitrary point of the body can be written by using the conservation law of linear momentum as

$$\sigma_{ij,j} + \rho f_i = \rho(z_{,tt})_i \quad (i, j = 1, 2, 3) \tag{1}$$

where the boundary and initial conditions are

$$\sigma_{ij} n_j = T_i(t) \quad \text{on } \Gamma_t \tag{2}$$

$$\mathbf{z}(\mathbf{X}, t) = \mathbf{d}(t) \quad \text{on } \Gamma_d \tag{3}$$

$$\mathbf{z}(\mathbf{X}, 0) = {}^{0}\mathbf{z} \quad \text{in } \Omega \tag{4}$$

and

$$\mathbf{z}_{,t}(\mathbf{X}, 0) = {}^{0}\mathbf{z}_{,t} \quad \text{in } \Omega \tag{5}$$

In the updated Lagrangian formulation, the previous configuration (n) is used as the reference frame. Using the updated Lagrangian formulation with simplified notations, the variational equation can be rewritten as

$$\int_{{}^{n}t}^{{}^{n+1}t} [d(\mathbf{z}_{,tt}, \bar{\mathbf{z}}) + a(\mathbf{z}, \bar{\mathbf{z}})]\,\mathrm{d}t = \int_{{}^{n}t}^{{}^{n+1}t} [\ell(\bar{\mathbf{z}})]\,\mathrm{d}t \quad \text{for all } \bar{\mathbf{z}} \in Z,\ t \in [{}^{n}t, {}^{n+1}t] \tag{6}$$

where

$$d(\mathbf{z}_{,tt}, \bar{\mathbf{z}}) \equiv \iiint_{{}^{n}\Omega} \rho^{n+1} (z_{,tt})_i \, {}^{n+1}\bar{\mathbf{z}}_i \,\mathrm{d}\Omega \tag{7}$$

$$a(\mathbf{z}, \bar{\mathbf{z}}) \equiv \iiint_{{}^{n}\Omega} {}^{n+1}\sigma_{ij} \, {}^{n+1}\bar{z}_{i,j} \,\mathrm{d}\Omega \tag{8}$$

$$\ell(\bar{\mathbf{z}}) \equiv \iiint_{{}^{n}\Omega} \rho^{n+1} f_i \, {}^{n+1}\bar{z}_i \,\mathrm{d}\Omega + \iiint_{{}^{n}\Gamma_t} {}^{n+1}T_i \, {}^{n+1}\bar{z}_i \,\mathrm{d}\Gamma_t \tag{9}$$

and f_i and T_i are external body force intensity and surface traction, respectively. Once the solution $\mathbf{z}_{,tt} \equiv {}^{n+1}\mathbf{z}_{,tt}$ is obtained from Equation (6), the remaining kinematic unknowns in the next time step can be computed using the central difference integrator that imposes dynamic equilibrium at the two end points of the finite time interval as

$${}^{n+1}\Delta t = {}^{n+1}t - {}^{n}t \tag{10}$$

$${}^{n+1/2}\mathbf{z}_{,t} = {}^{n-1/2}\mathbf{z}_{,t} + {}^{n}\Delta t \, {}^{n}\mathbf{z}_{,tt} \tag{11}$$

and

$${}^{n+1}\mathbf{z} = {}^{n}\mathbf{z} + \tfrac{1}{2}({}^{n}\Delta t + {}^{n+1}\Delta t)^{n+1/2}\mathbf{z}_{,t} \tag{12}$$

2.1. Element formulation

To treat finite strain and rotation, it is necessary to use appropriate stress and strain measures, stress integration scheme and element formulation. The rate of deformation tensor and the Jaumann rate-based stress integration scheme have desirable objectivity to handle finite rotation problems. The Hughes–Liu beam element has several desirable features such that it is incrementally objective, allowing for the treatment of finite strains including finite transverse shear strains. Consider the solid element with an isoparametric mapping of the bi-unit cube as shown in Figure 1.

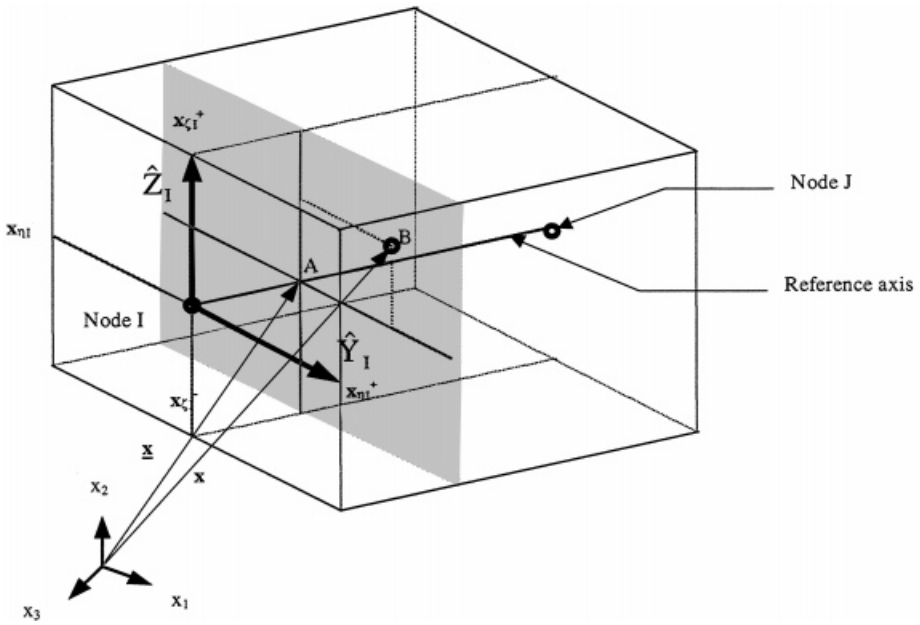

Figure 1. Hughes–Liu beam element.

A point **x** in the element can be interpolated using the global nodal co-ordinates of node I and the element shape functions evaluated at node I [12, 13] as

$$\begin{aligned}\mathbf{x}(\xi,\eta,\zeta) &= N_{\mathrm{I}}(\xi)\underline{\mathbf{x}}_{\mathrm{I}} + N_{\mathrm{I}}(\xi)\tfrac{1}{2}\{(1+\eta)z_{\eta\mathrm{I}}^{+} + (1-\eta)z_{\eta\mathrm{I}}^{-}\}\hat{\mathbf{Y}}_{\mathrm{I}} + N_{\mathrm{I}}(\xi)\tfrac{1}{2}\{(1+\zeta)z_{\zeta\mathrm{I}}^{+} + (1-\zeta)z_{\zeta\mathrm{I}}^{-}\}\hat{\mathbf{Z}}_{\mathrm{I}}\\ &= N_{\mathrm{I}}(\xi)\underline{\mathbf{x}}_{\mathrm{I}} + N_{\mathrm{I}}(\xi)\tfrac{1}{4}\{(1+\eta)(1-\eta_{\mathrm{I}})\|\mathbf{x}_{\eta\mathrm{I}}^{+} - \mathbf{x}_{\eta\mathrm{I}}^{-}\| - (1-\eta)(1+\eta_{\mathrm{I}})\|\mathbf{x}_{\eta\mathrm{I}}^{+} - \mathbf{x}_{\eta\mathrm{I}}^{-}\|\}\hat{\mathbf{Y}}_{\mathrm{I}}\\ &\quad + N_{\mathrm{I}}(\xi)\tfrac{1}{4}\{(1+\zeta)(1-\zeta_{\mathrm{I}})\|\mathbf{x}_{\zeta\mathrm{I}}^{+} - \mathbf{x}_{\zeta\mathrm{I}}^{-}\| - (1-\zeta)(1+\zeta_{\mathrm{I}})\|\mathbf{x}_{\zeta\mathrm{I}}^{+} - \mathbf{x}_{\zeta\mathrm{I}}^{-}\|\}\hat{\mathbf{Z}}_{\mathrm{I}}\\ &= N_{\mathrm{I}}(\xi)\underline{\mathbf{x}}_{\mathrm{I}} + N_{\mathrm{I}}(\xi)\tfrac{1}{2}(\eta-\eta_{\mathrm{I}})\|\mathbf{x}_{\eta\mathrm{I}}^{+} - \mathbf{x}_{\eta\mathrm{I}}^{-}\|\hat{\mathbf{Y}}_{\mathrm{I}} + N_{\mathrm{I}}(\xi)\tfrac{1}{2}(\zeta-\zeta_{\mathrm{I}})\|\mathbf{x}_{\zeta\mathrm{I}}^{+} - \mathbf{x}_{\zeta\mathrm{I}}^{-}\|\hat{\mathbf{Z}}_{\mathrm{I}} \end{aligned} \tag{13}$$

where $N_{\mathrm{I}}(\xi) = \frac{1}{2}(1+\xi\xi_{\mathrm{I}})$ is the one-dimensional shape function, $\mathbf{x}_{\mathrm{I}}$ the position vector on the reference axis at node I, $\hat{\mathbf{Y}}_{\mathrm{I}}$, $\hat{\mathbf{Z}}_{\mathrm{I}}$ are unit fibre vectors in y- and z-directions at node I, $z_{\eta\mathrm{I}}^{+}$, $z_{\eta\mathrm{I}}^{-}$, $z_{\zeta\mathrm{I}}^{+}$, $z_{\zeta\mathrm{I}}^{-}$ are thickness function evaluated at the top and bottom surfaces and $\mathbf{x}_{\eta\mathrm{I}}^{+}$, $\mathbf{x}_{\eta\mathrm{I}}^{-}$, $\mathbf{x}_{\zeta\mathrm{I}}^{+}$, $\mathbf{x}_{\zeta\mathrm{I}}^{-}$ are position vectors located at the top and bottom surfaces.

In the Hughes–Liu beam element, the displacements of the reference axis and the rotations of the fibre vectors characterize the deformation and finite strains including finite transverse shear strain. The displacements are obtained using the Newton–Euler equation. The rotation matrix **R** to update the fibre vectors can be obtained using the rotational displacements and the Hughes–Winget algorithm [13, 14]. The rotation matrix **R** is second-order accurate and incrementally objective as

$$\mathbf{R} = (\mathbf{I} - \gamma\mathbf{W})^{-1}[\mathbf{I} + (1-\gamma)\mathbf{W}] \tag{14}$$

and

$$\mathbf{W} = \begin{bmatrix} 0 & -\Delta z_6 & \Delta z_5 \\ \Delta z_6 & 0 & -\Delta z_4 \\ -\Delta z_5 & \Delta z_4 & 0 \end{bmatrix} = \Delta\omega = \int_{n_t}^{n+1_t} \omega \, \mathrm{d}t \tag{15}$$

where Δz_4, Δz_5, and Δz_6 are incremental rotational displacements in global Cartesian coordinates, and ω and γ are a spin tensor and a parameter in the generalized midpoint rule for integration, respectively. The updated unit fibre vectors can be obtained as

$$^{n+1}\hat{\mathbf{Y}} = \mathbf{R}^n \hat{\mathbf{Y}} \tag{16}$$

and

$$^{n+1}\hat{\mathbf{Z}} = \mathbf{R}^n \hat{\mathbf{Z}} \tag{17}$$

2.2. Stress integration

For the finite rotation, it is necessary to choose the appropriate stress and strain measures and the stress integration scheme that have objectivity characteristics. In this paper, Jaumann rate of Cauchy stress, rate of deformation tensor, and Jaumann rate based incrementally objective stress integration scheme are used. The stress of the elastic–plastic material is integrated incrementally in time so that

$$\sigma_{ij}(t + \mathrm{d}t) = \sigma_{ij}(t) + \dot{\sigma}_{ij}(t)\,\mathrm{d}t \tag{18}$$

The material time derivative of the stress tensor is given by

$$\dot{\sigma}_{ij} = \sigma_{ij}^{\nabla} + \sigma_{ik}\omega_{kj} + \sigma_{jk}\omega_{ki} \tag{19}$$

where the Jaumann stress rate is given by

$$\sigma_{ij}^{\nabla} = C_{ijkl}\dot{\varepsilon}_{kl} \tag{20}$$

and C_{ijkl} is the stress-dependent constitutive matrix.

3. SIZING DESIGN SENSITIVITY ANALYSIS AND OPTIMIZATION

3.1. Sizing design sensitivity formulation

The mathematical theory of the differentiability of non-linear structural responses has not yet been well developed in the literature, whereas a reasonably complete theory of the differentiability of linear structural responses is given in Reference [15]. Thus, the differentiability is assumed in deriving design sensitivity expressions in this paper. Consider the equations of motion

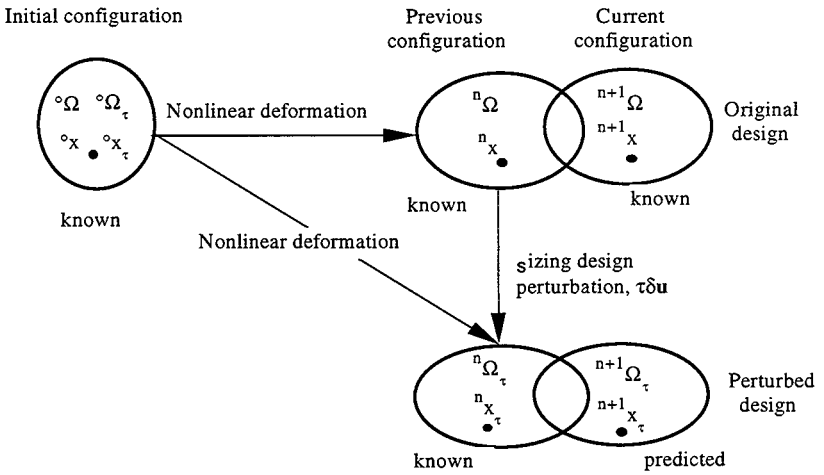

Figure 2. Deformation of body with sizing design perturbation.

corresponding to the original design $\mathbf{u}$ and the perturbed design $\mathbf{u} + \tau\delta\mathbf{u}$, at the current configuration $(n + 1)$, as

$$d_u(\mathbf{z}_{,tt}, \bar{\mathbf{z}}) + a_u(\mathbf{z}, \bar{\mathbf{z}}) = \ell_u(\bar{\mathbf{z}}) \quad \text{for all } \bar{\mathbf{z}} \in Z \tag{21}$$

and

$$d_{u+\tau\delta u}((\mathbf{z}_{,tt})_\tau, \bar{\mathbf{z}}_\tau) + a_{u+\tau\delta u}(\mathbf{z}_\tau, \bar{\mathbf{z}}_\tau) = \ell_{u+\tau\delta u}(\bar{\mathbf{z}}_\tau) \quad \text{for all } \bar{\mathbf{z}}_\tau \in Z \tag{22}$$

Equations (21) and (22), with Figure 2 showing the schematic of deformation for the original and the perturbed designs, state that the difference of the response between the original and perturbed designs is small for a small design perturbation $\tau\delta\mathbf{u}$. Hence, as the design perturbation vanishes, so does the difference in the responses.

The first-order variations of each term in Equation (21) with respect to its explicit dependence on the design variable $\mathbf{u}$ are defined as

$$d'_{\delta u}(\tilde{\mathbf{z}}_{,tt}, \bar{\mathbf{z}}) \equiv \frac{\mathrm{d}}{\mathrm{d}\tau} d_{u+\tau\delta u}((\tilde{\mathbf{z}}_{,tt})_\tau, \bar{\mathbf{z}}_\tau)|_{\tau=0} \tag{23}$$

$$a'_{\delta u}(\tilde{\mathbf{z}}, \bar{\mathbf{z}}) \equiv \frac{\mathrm{d}}{\mathrm{d}\tau} a_{u+\tau\delta u}(\tilde{\mathbf{z}}_\tau, \bar{\mathbf{z}}_\tau)|_{\tau=0} \tag{24}$$

and

$$\ell'_{\delta u}(\bar{\mathbf{z}}) \equiv \frac{\mathrm{d}}{\mathrm{d}\tau} \ell_{u+\tau\delta u}(\bar{\mathbf{z}}_\tau)|_{\tau=0} \tag{25}$$

where the ' $\sim$ ' denotes that the dependence on the design variation is suppressed and the virtual displacement $\bar{\mathbf{z}}$ is independent of τ. Note that both the kinetic energy form $[d(\mathbf{z}_{,tt}, \bar{\mathbf{z}})]$ and the load form $[\ell(\bar{\mathbf{z}})]$ are linear with respect to their arguments. However, the strain energy form $[a(\mathbf{z}, \bar{\mathbf{z}})]$ is non-linear due to the finite strain and rotation, and the material non-linearity. The first-order variations of the solution $\mathbf{z}_{,tt}$ of Equation (21) and the response $\mathbf{z}$ with respect to the sizing design variable $\mathbf{u}$ are defined as

$$\mathbf{z}'_{,tt} \equiv \frac{\mathrm{d}}{\mathrm{d}\tau}\mathbf{z}_{,tt}(\mathbf{u} + \tau\delta\mathbf{u})|_{\tau=0} = \lim_{\tau\to 0}\frac{\mathbf{z}_{,tt}(\mathbf{u} + \tau\delta\mathbf{u}) - \mathbf{z}_{,tt}(\mathbf{u})}{\tau} \tag{26}$$

and

$$\mathbf{z}' \equiv \frac{\mathrm{d}}{\mathrm{d}\tau}\mathbf{z}(\mathbf{u} + \tau\delta\mathbf{u})|_{\tau=0} = \lim_{\tau\to 0}\frac{\mathbf{z}(\mathbf{u} + \tau\delta\mathbf{u}) - \mathbf{z}(\mathbf{u})}{\tau} \tag{27}$$

Using the above notation, since the co-ordinates and the design variation parameter τ are independent variables, the order of taking the first-order variation and the partial derivative of the response can be interchanged as $(\mathbf{z}_{,i})' = (\mathbf{z}')_{,i}$ [1]. Using the chain rule of differentiation and Equations (23)–(25), the first-order variation of each term in Equation (21) becomes

$$\frac{\mathrm{d}}{\mathrm{d}\tau}d_{u+\tau\delta u}(\mathbf{z}_{,tt}(\mathbf{u} + \tau\delta\mathbf{u}), \bar{\mathbf{z}}_\tau)|_{\tau=0} = d'_{\delta u}(\tilde{\mathbf{z}}_{,tt}, \bar{\mathbf{z}}) + d_u(\mathbf{z}'_{,tt}, \bar{\mathbf{z}}) \tag{28}$$

$$\frac{\mathrm{d}}{\mathrm{d}\tau}a_{u+\tau\delta u}(\mathbf{z}(\mathbf{u} + \tau\delta\mathbf{u}), \bar{\mathbf{z}}_\tau)|_{\tau=0} = a'_{\delta u}(\tilde{\mathbf{z}}, \bar{\mathbf{z}}) + a^*_z(\mathbf{z}; \mathbf{z}', \bar{\mathbf{z}}) \tag{29}$$

and

$$\frac{\mathrm{d}}{\mathrm{d}\tau}\ell_{u+\tau\delta u}(\bar{\mathbf{z}}_\tau)|_{\tau=0} = \ell'_{\delta u}(\bar{\mathbf{z}}) \tag{30}$$

Taking the first-order variation of Equation (21) yields

$$d'_{\delta u}(\tilde{\mathbf{z}}_{,tt}, \bar{\mathbf{z}}) + d_u(\mathbf{z}'_{,tt}, \bar{\mathbf{z}}) + a'_{\delta u}(\tilde{\mathbf{z}}, \bar{\mathbf{z}}) + a^*_u(\mathbf{z}; \mathbf{z}', \bar{\mathbf{z}}) = \ell'_{\delta u}(\bar{\mathbf{z}}) \quad \text{for all } \bar{\mathbf{z}} \in \mathbf{Z} \tag{31}$$

where $a^*_u(\mathbf{z}; \mathbf{z}', \bar{\mathbf{z}})$ represents that the first-order differentiation is taken for the non-linear argument $\mathbf{z}$. The explicit form of the variational Equation (31) can be obtained, in the absence of the traction loading for simplicity, using the definition of the energy and load forms of Equations (7)–(9) as

$$\left[\iiint_\Omega \rho(\tilde{z}_{,tt})_i \bar{z}_i \,\mathrm{d}\Omega\right]'_{\delta u} + \iiint_\Omega \rho(z_{,tt})'_i \bar{z}_i \,\mathrm{d}\Omega + \left[\iiint_\Omega \sigma_{ij}(\tilde{\mathbf{z}})\bar{z}_{i,j}\,\mathrm{d}\Omega\right]'_{\delta u}$$
$$+ \iiint_\Omega \sigma_{ij_u}(\mathbf{z}; \mathbf{z}')\bar{z}_{i,j}\,\mathrm{d}\Omega = \left[\iiint_\Omega \rho f_i \bar{z}_i \,\mathrm{d}\Omega\right]'_{\delta u} \tag{32}$$

3.2. Design sensitivity of structural responses

To obtain the stress sensitivity, consider the elastic–plastic material model proposed by Kreg and Key [11]. If material properties E and E_p are used alternatively depending on the state of the stress, the stress sensitivity expression may be discontinuous [4]. Hence, a unified stress expression is desirable to represent both states of the stress to avoid this difficulty. The trial stress σ^* for the radial return algorithm can be written as

$$\sigma_{ij}^* = {}^n\sigma_{ij} + C_{ijkl}\Delta\varepsilon_{kl} \tag{33}$$

Also, the trial deviatoric stress χ^* can be determined by

$$\chi_{ij}^* = \sigma_{ij}^* - \tfrac{1}{3}\sigma_{kk}^* - \alpha_{ij} \tag{34}$$

where α is a back-stress tensor.

In elastic state, the stress σ_{ij} depends only on the state of strain. However, beyond the yield stress σ_y, non-recoverable plastic deformation occurs. The yield function that describes the pressure-independent yield surface is the function of the deviatoric stress tensor as

$$Y = \Lambda^2 - \sigma_y^2 \tag{35}$$

where

$$\Lambda^2 = \tfrac{3}{2}\chi_{ij}\chi_{ij} \tag{36}$$

and

$$\sigma_y = \sigma_0 + (1-\beta)E_p\varepsilon_{\text{eff}}^p \tag{37}$$

and σ_0 and σ_y are the initial and the current yield stresses, respectively; and the parameter β is equal to one for kinematic hardening and zero for isotropic hardening. Also, the plastic hardening modulus and the effective plastic strain are defined, respectively, as

$$E_p \equiv \frac{EE_t}{E - E_t} \tag{38}$$

and

$$\varepsilon_{\text{eff}}^p \equiv \int_0^t \left(\frac{2}{3}\dot{\varepsilon}_{ij}^p\dot{\varepsilon}_{ij}^p\right)^{1/2} \mathrm{d}t \tag{39}$$

where $\dot{\varepsilon}^p$ is the plastic part of strain rate tensor.

If the state is elastic (i.e. $Y \leqslant 0$), the trial stresses are accepted. Otherwise, in the plastic state, the effective plastic strain is computed and the stress deviator is scaled back using a return mapping algorithm and the von Mises yield criterion. The additive decomposition of the strains and the plane stress plasticity are assumed in this material model. The application of the Jaumann rate to update the stress raises the possibility that the normal stress may not be equal to zero.

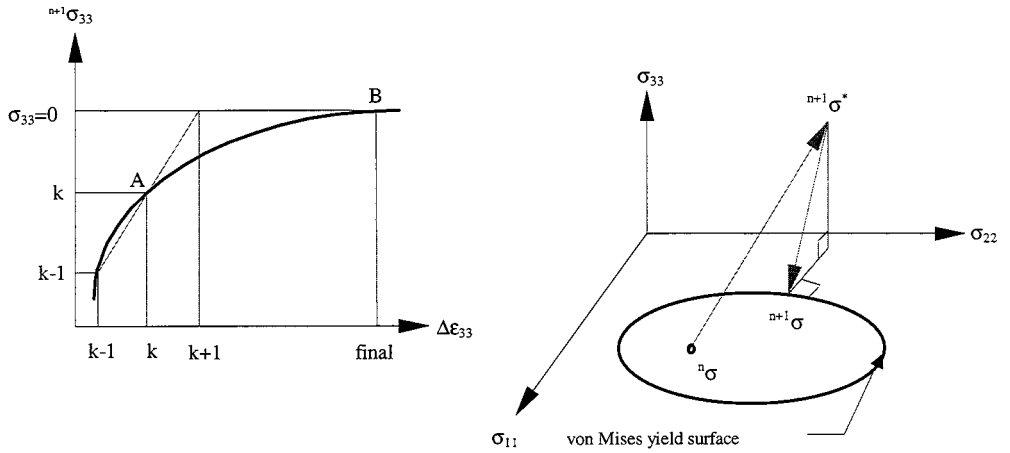

Figure 3. Secant iteration for plane plasticity.

Therefore, to update the stress in the plastic state, the secant iteration method is used during the return mapping [17] to enforce the condition that the normal strain increment produces zero normal stress.

The secant iteration method shown in Figure 3 is described by

$$ {}^{n+1}\sigma_{33}^{k} = {}^{n+1}\sigma_{33}^{k*} - (\Delta\varepsilon_{\text{eff}}^{\text{P}})^{k}\frac{3G}{\Lambda^{k}}\,{}^{n+1}\chi_{33}^{k} \tag{40} $$

$$ (\Delta\varepsilon_{\text{eff}}^{\text{P}})^{k} = \frac{\Lambda^{k} - \sigma_{\text{y}}^{k}}{3G + E_{\text{p}}} \tag{41} $$

and

$$ \Delta\varepsilon_{33}^{k+1} = \Delta\varepsilon_{33}^{k} - {}^{n+1}\sigma_{33}^{k}\frac{\Delta\varepsilon_{33}^{k} - \Delta\varepsilon_{33}^{k-1}}{\sigma_{33}^{k} - \sigma_{33}^{k-1}} \tag{42} $$

where the two starting values, $\Delta\varepsilon_{33}^{k}$ and $\Delta\varepsilon_{33}^{k-1}$, are obtained from the initial elastic estimate and by assuming a purely plastic increment. That is

$$ \Delta\varepsilon_{33}^{k} = \Delta\varepsilon_{22}^{k} = -\tfrac{1}{2}\Delta\varepsilon_{11}^{k} \tag{43} $$

Once $\Delta\varepsilon^{k}$, point A in Figure 3, is initially obtained using the stress-dependent constitutive relation, σ_{33}^{k} is determined using Equations (40) and (41). If $|\sigma_{33}^{k}|$ is larger than specified tolerance, $\Delta\varepsilon^{k+1}$ for the next iteration $(k+1)$ is determined by Equation (42). The iteration proceeds to point B until ${}^{n+1}\sigma_{33}$ is sufficiently small. Finally, the stresses are determined by

$$ {}^{n+1}\sigma_{ij} = {}^{n+1}\sigma_{ij}^{*\text{final}} - (\Delta\varepsilon_{\text{eff}}^{\text{P}})^{\text{final}}\frac{3G}{\Lambda^{\text{final}}}\,{}^{n+1}\chi_{ij}^{\text{final}} \tag{44} $$

and

$$ {}^{n+1}\alpha_{ij} = {}^{n+1}\alpha_{ij}^{*\text{final}} + (1-\beta)\,E_{\text{P}}(\Delta\varepsilon_{\text{eff}}^{P})^{\text{final}}\,\frac{1}{\Lambda^{\text{final}}}\,{}^{n+1}\chi_{ij}^{\text{final}} \tag{45} $$

The stresses in Equations (44) and (45) are written in a unified expression to represent both states of the stresses. The first-order variations of Equations (44) and (45) are taken to obtain the stress sensitivities as

$$ \begin{aligned} {}^{n+1}\sigma'_{ij} = {}^{n+1}\sigma'^{*\text{final}}_{ij} - \frac{3G}{(\Lambda^{\text{final}})^2}\{&[(\Delta\varepsilon_{\text{eff}}^{\text{P}})'^{\text{final}\,n+1}\chi_{ij}^{\text{final}} + (\Delta\varepsilon_{\text{eff}}^{\text{P}})^{\text{final}\,n+1}\chi'^{\text{final}}_{ij}]\,\Lambda^{\text{final}} \\ &- (\Delta\varepsilon_{\text{eff}}^{\text{P}})^{\text{final}\,n+1}\chi_{ij}^{\text{final}}\Lambda'^{\text{final}}\} \end{aligned} \tag{46} $$

$$ \begin{aligned} {}^{n+1}\alpha'_{ij} = {}^{n+1}\alpha_{ij}^{*\text{final}} + \frac{(1-\beta)\,E_{\text{P}}}{(\Lambda^{\text{final}})^2}\{&[(\Delta\varepsilon_{\text{eff}}^{\text{P}})'^{\text{final}\,n+1}\chi_{ij}^{\text{final}} + (\Delta\varepsilon_{\text{eff}}^{\text{P}})^{\text{final}\,n+1}\chi'^{\text{final}}_{ij}]\,\Lambda^{\text{final}} \\ &- (\Delta\varepsilon_{\text{eff}}^{\text{P}})^{\text{final}\,n+1}\chi_{ij}^{\text{final}}\Lambda'^{\text{final}}\} \end{aligned} \tag{47} $$

where necessary variations can be computed by taking the first-order variations of the previous Equations (33)–(43) according to the procedure of stress determination.

3.3. Design sensitivity of kinematic responses

Once the solution $\{{}^{n+1}\mathbf{z}_{,tt}\}'$ of Equation (32) is obtained, the sensitivities of the other kinematic response are found using the central difference method as

$$ ({}^{n+1/2}\mathbf{z}_{,t})' = ({}^{n-1/2}\mathbf{z}_{,t})' + {}^{n}\Delta t\,({}^{n}\mathbf{z}_{,tt})' + ({}^{n}\Delta t)'\,{}^{n}\mathbf{z}_{,tt} \tag{48} $$

and

$$ ({}^{n+1}\mathbf{z})' = ({}^{n}\mathbf{z})' + \tfrac{1}{2}({}^{n}\Delta t + {}^{n+1}\Delta t)({}^{n+1/2}\mathbf{z}_{,t})' + \tfrac{1}{2}({}^{n}\Delta t + {}^{n+1}\Delta t)'^{n+1/2}\,\mathbf{z}_{,t} \tag{49} $$

Note that the time step ${}^{n}\Delta t$ is determined by its geometric and material properties. To obtain kinematic responses in Equations (48) and (49), ${}^{n+1}\Delta t$ should be less than the critical time step that is determined by the material property and the element length as [16]

$$ \begin{aligned} {}^{n+1}\Delta t &= \kappa\sqrt{\frac{3\rho}{3K+4G}}\,{}^{n}\ell \\ &= \kappa\sqrt{\frac{3\rho}{3K+4G}\sum_{i=1}^{3}[({}^{0}x_i + {}^{n}z_i)_J - ({}^{0}x_i + {}^{n}z_i)_I]^2} \end{aligned} \tag{50} $$

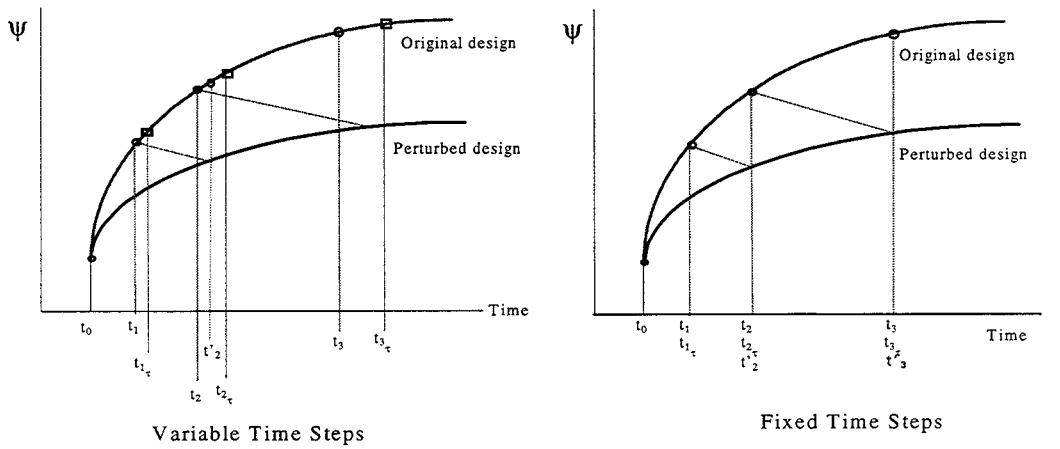

Figure 4. Performance measures with variable and fixed time steps.

where κ and ${}^0\mathbf{x}$ are the initial geometry and time step scale factor, respectively. I and J represent the node numbers of the critical element. The design sensitivity of the time step is written as

$$({}^{n+1}\Delta t)'_{\delta u} = \kappa \sqrt{\frac{3\rho}{3K+4G}}({}^n\ell)'_{\delta u}$$

$$= \kappa \sqrt{\frac{3\rho}{3K+4G}} \frac{\sum_{i=1}^{3} [({}^0x_i + {}^nz_i)_J - ({}^0x_i + {}^nz_i)_I][\{({}^nz_i)'_{\delta u}\}_J - \{({}^nz_i)'_{\delta u}\}_I]}{{}^n\ell} \tag{51}$$

The design sensitivity of the time step will not predict the exact perturbation. Thus, there is a slight difference between the predicted time steps (t') and the actual time steps (t_τ) for the perturbed design, as shown in Figure 4. Even though the difference is small, the error in the time step will accumulate inaccuracy of the design sensitivity of the structural response. This is especially true for the explicit method. To avoid this difficulty, one can use a small fixed time step that is less than the critical time step for analysis. In this case, the design sensitivity of time steps given in Equation (51) is not necessary. This will be discussed later in numerical examples.

3.4. Direct differentiation method

In the path-dependent problem, the state of stresses and plastic strains at a given time depends on the full history of state variables. The response sensitivity at a given time and position depends on both the response and the response sensitivities of all previous times and locations of the structure. In other words, the exact paths of the response and its sensitivity are needed. Thus the adjoint variable method is not appropriate for the path-dependent problem because each adjoint solution yields the sensitivity of only one performance measure, rather than the sensitivities of the full response fields. Therefore, the direct differentiation method is employed in this paper.

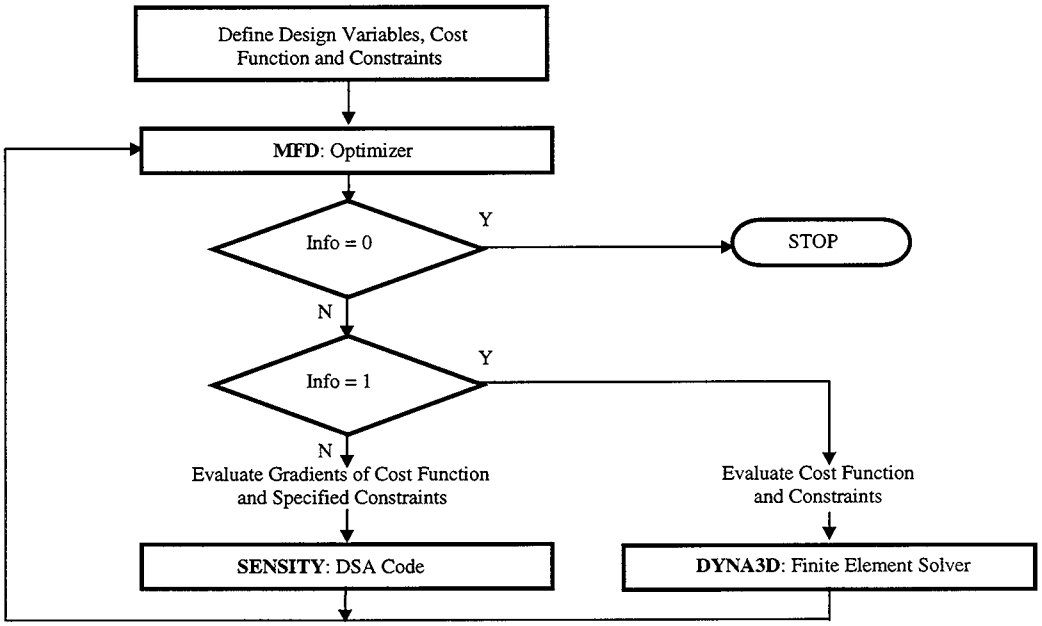

Figure 5. Optimization loop.

3.5. *Design optimization*

A general optimal design problem can be formulated as

$$\min_{\mathbf{b}} \psi(\mathbf{b}) \tag{52}$$

subject to constraints

$$\mathbf{c} = \mathbf{s} - \mathbf{s}_0 \leqslant \mathbf{0} \tag{53}$$

and design variable bounds

$$\mathbf{b}_\ell \leqslant \mathbf{b} \leqslant \mathbf{b}_u \tag{54}$$

where ψ is the cost function and $\mathbf{b}$, $\mathbf{b}_\ell$, and $\mathbf{b}_u$ are design variables and their lower and upper bounds, respectively. Also, $\mathbf{s}$ and $\mathbf{s}_0$ are constraints and specified limitations, respectively. The design problem of Equations (52)–(54) can be solved using a gradient-based mathematical programming algorithm. The flow chart of the general optimization procedure is given in Figure 5.

The design variables, cost function and constraints are provided to the optimizer. If the control parameter 'info' is equal to zero, the optimization is completed. If info = 1, the cost function and

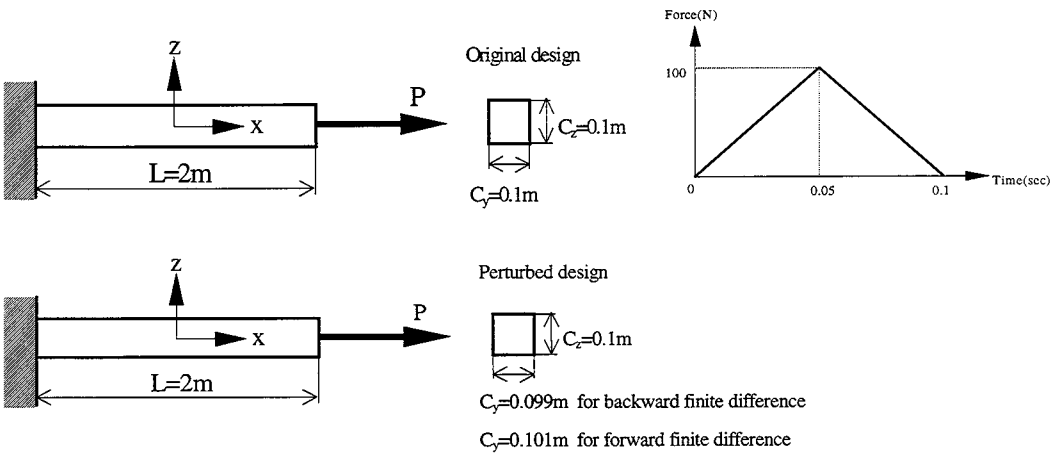

Figure 6. Original and perturbed designs.

constraints are evaluated. If info = 2, the gradient of the cost function and the constraints are evaluated. The proposed DSA method is used to obtain the required gradient information. This process continues until the desired optimum design is obtained. The optimization is carried out using the method of feasible direction (MFD) along with the one-dimensional search algorithm that first finds bounds and then uses polynomial interpolation. The feasible direction is determined such that, for a sufficiently small step size, the new design is feasible and the new cost function is smaller than the old one. Once the feasible direction is found, the one-dimensional search is performed to determine the step size along the feasible direction. For one-dimensional search, the zero-order method such as equal interval search is inefficient for many practical problems. A continuous function on a given interval can be approximated by passing a sufficiently high-order polynomial. The minimum point of the approximating polynomial is often a good estimate of the exact minimum of the one-dimensional search function.

4. NUMERICAL EXAMPLES

4.1. Sizing design sensitivity of cantilever

The purpose of this example is to demonstrate effects of the variable integration time step to the accuracy of the design sensitivity. The dimensions of the original and the perturbed designs, and boundary conditions are shown in Figure 6. The elastic–plastic material model with the linear isotropic hardening assumption is used. The MKS unit is used for all numerical examples.

The design sensitivity results are compared with the results of the central finite differences. To make the time-step size large enough to be within the significant digits of the single precision (7–8 digits), a fictitious material is assumed. Young's modulus, density, and Poisson ratio are 20 000, 50 000 and 0.3, respectively. In Table I, the time steps and their sensitivities are presented at the initial and the final (70th) time steps. Note that the final time step is noticeably different from the initial one and the sensitivities of the time steps are not small.

Table I. Comparison of time steps and sensitivities.

	Initial	Final
Δt	0.136277E + 01	0.143058E + 01
$(\Delta t)'_{\delta u}$	− 0.344898E − 02	− 0.693570E + 00

Table II. Comparison of DSA accuracy of stress performance measure.

	Single precision		Double precision	
Time steps	Variable	Fixed	Variable	Fixed
10	100.47	99.96	100.46	99.97
20	100.94	99.95	100.93	99.94
30	101.47	99.92	101.47	99.91
40	102.15	99.88	102.16	99.87
50	103.15	99.88	103.16	99.82
60	104.76	99.73	104.89	99.76
70	108.76	99.54	109.15	99.64

If fixed time step is employed in non-linear finite element analysis, then DSA of the time step is not necessary.

The results in Table II indicate that the variable time step affects the accuracy of design sensitivity results, even though DSA of the time step is applied to obtain the design sensitivity of the stress.

The same example is tested using steel with $E = 2.0\text{E} + 11\ (\text{N/m}^2)$, $\rho = 7.8\text{E} + 03\ (\text{kg/m}^2)$, and $v = 0.3$. In Table III, the time steps and their sensitivities are presented at the initial and final (500th) time steps. Note that the difference between the initial and the final time steps is very small and the sensitivities of these time steps are insignificant.

Results in Table IV indicate that the effects of the variable time steps are not significant because the time steps are not varying significantly during analysis. More over, better sensitivity results are obtained when the double precision is used. The result of this example suggests that the best combination is to use double precision and a fixed time step for both analysis and DSA.

4.2. Sizing design sensitivity of vehicle frame

Consider a steel vehicle frame structure shown in Figure 7, where finite strain and rotation effects are considered. The kinematic responses at selected nodes of the longitudinal components are selected as performance measures. The finite element model consists of 48 beam elements. To verify the accuracy of the design sensitivity, some of the longitudinal and the cross components are perturbed by 1 per cent as shown in Table V, where C_y and C_z are the cross-sectional dimensions of the rectangular beam. Analysis with 118 load steps is performed under the impact loading (like the one in Figure 6 with the maximum load of 10^4 kN) for the duration of 2000 μs. The deformed shape is shown in Figure 7 at selected time steps.

Table III. Comparison of time steps and sensitivities.

	Initial	Final
Δt	0.170210E − 03	0.170210E − 03
$(\Delta t)'_{\delta u}$	− 0.538410E − 13	− 0.720552E − 10

Table IV. Comparison of DSA accuracy of stress performance measure.

	Single precision		Double precision	
Time steps	Variable	Fixed	Variable	Fixed
10	99.99	99.99	99.99	99.99
100	99.96	99.96	99.99	99.99
200	99.99	99.99	99.99	99.99
300	95.59	95.59	99.99	99.99
400	100.12	100.12	99.99	99.99
500	100.56	100.56	99.99	99.99

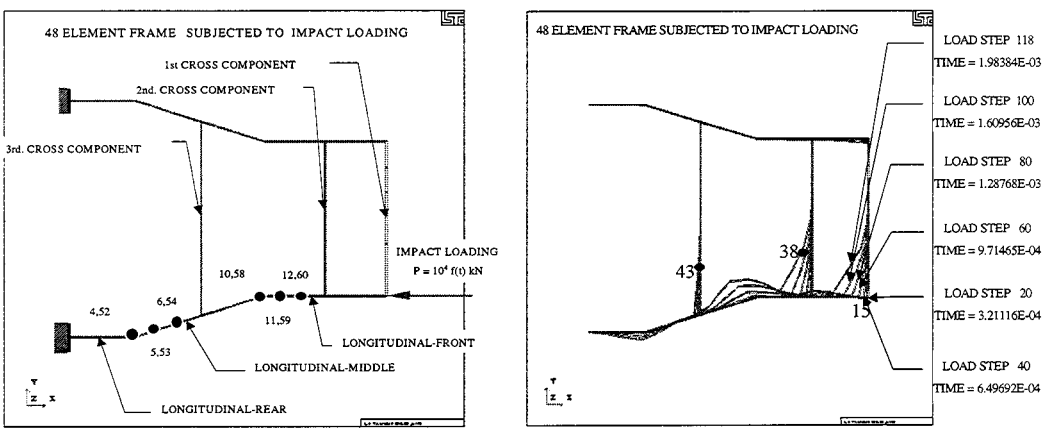

Figure 7. Initial design and deformed shapes of vehicle frame.

The transient history of the design sensitivities of acceleration is shown in Table VI for selected nodes and time steps. It is noted in this problem that the acceleration is more sensitive with respect to the design than the velocity and displacement. Also, it is noted that the sensitivities of the displacement and velocity are more accurate than the sensitivity of the acceleration. In this table, $\delta\psi$ represents the predicted variation using the proposed DSA method; $\Delta\psi$ represents the finite difference result; and $\delta\psi/\Delta\psi$ stands for the agreement of the predicted variation with respect to the finite difference result. In Table VI, the sensitivity of the y-acceleration at node 40 yields 90.41 per cent agreement at load step 40 but improves to 98.46 per cent at time step 70, which

Table V. Perturbed components for sizing DSA of vehicle frame.

Description of component	Element	Pert. of C_y (%)	Pert. of C_z (%)
Longitudinal-middle	4, 5, 6, 7, 8, 9	1.000	0.000
Longitudinal-front	10, 11, 12, 13, 14, 15	0.000	1.000
Second cross component	37, 38, 39, 40, 41, 42	1.000	1.000
Third cross component	43, 44, 45, 46, 47, 48	1.000	1.000

implies that analytical sensitivity provides better sensitivity results than the finite difference for the highly non-linear problem. If the analytical sensitivities were inaccurate, the error should have been accumulated at later load steps. In Table VII, the sensitivities of the shear stress at element 1 yields around 110 per cent agreement but are improved at later load steps, which also implies that the analytical DSA method yields better sensitivity results.

4.3. Sizing design optimization of vehicle frame

The vehicle frame model needs to be designed to absorb as much energy as possible and to transfer less energy to the passenger in the event of crash or impact situation. The design objective is as follows: determine the cross-sectional dimensions of structural components, subject to kinematic and structural limitations such that the specified acceleration levels are minimized and the specified responses meet the prescribed criteria.

Based on the finite element analysis results of the initial design, the cost function, constraints, and design variables are selected to improve the response at some specified location and time. The cost function, which is the total translational acceleration at the specified location and time, is defined as

$$\psi(\mathbf{b}) = \sqrt{\sum_{i=1}^{3} ({}^{n}z_{i,tt})_m^2} \tag{55}$$

which is computed at node $m = 43$ and load step $n = 118$. Also, the normalized constraint vector $\mathbf{c}$ is defined as

$$c_1 = -\frac{({}^{95}z_{1,tt})_{43}}{7.0 \times 10^4} - 1.0 \tag{56}$$

$$c_2 = \frac{({}^{110}z_{2,tt})_{43}}{7.0 \times 10^4} - 1.0 \tag{57}$$

and

$$c_3 = \frac{1}{4.0 \times 10^2} \sum_{i=1}^{\mathrm{ne}} d_i^s d_i^t \ell_i - 1.0 \tag{58}$$

Table VI. History of acceleration variation for sizing DSA of vehicle frame.

Load	Node	X-$\delta\psi$	Y-$\delta\psi$	Z-$\delta\psi$	X-$\Delta\psi$	Y-$\Delta\psi$	Z-$\Delta\psi$	X-$\delta\psi/\Delta\psi$	Y-$\delta\psi/\Delta\psi$	Z-$\delta\psi/\Delta\psi$
40	4	0.352196D + 03	0.146095D + 03	− 0.146806D + 03	0.352089D + 03	0.146059D + 03	− 0.146770D + 03	100.03	100.02	100.02
	6	0.125376D + 04	0.153969D + 03	− 0.380134D + 03	0.125495D + 04	0.154053D + 03	− 0.380279D + 03	99.90	99.95	99.96
	52	− 0.100478D + 01	0.188312D + 03	0.184234D + 03	− 0.100762D + 01	0.188535D + 03	0.184434D + 03	99.72	99.88	99.89
	54	− 0.452294D + 03	− 0.863794D + 01	− 0.151563D + 04	− 0.452383D + 03	− 0.955376D + 01	− 0.151683D + 04	99.98	**90.41**	99.92
70	4	− 0.890262D + 03	0.286738D + 04	− 0.252918D + 04	− 0.882564D + 03	0.287105D + 04	− 0.253262D + 04	100.87	99.87	99.86
	6	− 0.706282D + 03	− 0.122787D + 03	− 0.462041D + 03	− 0.701525D + 03	− 0.125900D + 03	− 0.457392D + 03	100.68	97.53	101.02
	52	0.757630D + 03	0.306891D + 04	0.558203D + 04	0.757918D + 03	0.306516D + 04	0.557929D + 04	99.96	100.12	100.05
	54	0.500331D + 03	− 0.274139D + 04	− 0.225288D + 04	0.501913D + 03	− 0.278436D + 04	− 0.227601D + 04	99.68	**98.46**	98.98
110	4	0.641833D + 04	− 0.935337D + 04	0.923883D + 04	0.631074D + 04	− 0.923569D + 04	0.913752D + 04	101.70	101.27	101.11
	6	0.130885D + 05	0.187790D + 04	− 0.592426D + 04	0.135265D + 05	0.198851D + 04	− 0.605878D + 04	96.76	94.44	97.78
	52	0.603457D + 04	− 0.176948D + 05	− 0.218121D + 05	0.603234D + 04	− 0.176301D + 05	− 0.214210D + 05	100.04	100.37	101.83
	54	− 0.109009D + 05	0.611409D + 04	− 0.223709D + 05	− 0.107913D + 05	0.532070D + 04	− 0.229336D + 05	101.02	114.91	97.55

Table VII. History of global stress variation for sizing DSA of vehicle frame.

Load	Elem	σ_{11}-$\delta\psi$	σ_{12}-$\delta\psi$	σ_{13}-$\delta\psi$	σ_{11}-$\Delta\psi$	σ_{12}-$\Delta\psi$	σ_{13}-$\Delta\psi$	σ_{11}-$\delta\psi/\Delta\psi$	σ_{12}-$\delta\psi/\Delta\psi$	σ_{13}-$\delta\psi/\Delta\psi$
40	**1**	0.193666D + 05	0.443090D + 02	− 0.400608D + 02	0.191829D + 05	0.401785D + 02	− 0.356526D + 02	100.96	**110.28**	**112.36**
	4	0.108491D + 07	0.309987D + 06	− 0.311716D + 06	0.108526D + 07	0.310061D + 06	− 0.311793D + 06	99.97	99.98	99.98
	17	− 0.835844D + 05	− 0.589407D + 06	0.902907D + 01	− 0.836059D + 05	− 0.589548D + 06	0.884195D + 01	99.97	99.98	102.12
	18	− 0.217869D + 04	− 0.275631D + 04	0.300073D + 02	− 0.217909D + 04	− 0.277040D + 04	0.300097D + 02	99.98	99.49	99.99
70	**1**	0.229054D + 08	− 0.137605D + 06	0.141141D + 06	0.229594D + 08	− 0.137932D + 06	0.141474D + 06	99.76	**99.76**	**99.76**
	4	0.334719D + 08	0.785888D + 07	− 0.726770D + 07	0.335118D + 08	0.786713D + 07	− 0.727539D + 07	99.88	99.90	99.89
	17	− 0.137913D + 07	− 0.630847D + 07	0.638194D + 05	− 0.138449D + 07	− 0.632129D + 07	0.640026D + 05	99.61	99.80	99.71
	18	− 0.896337D + 05	− 0.123101D + 07	0.416486D + 04	− 0.890443D + 05	− 0.122558D + 07	0.402503D + 04	100.66	100.44	103.47
110	1	− 0.604567D + 08	0.985217D + 07	− 0.100275D + 08	− 0.604288D + 08	0.100179D + 08	− 0.101572D + 08	100.05	98.35	98.72
	4	− 0.637014D + 08	− 0.249843D + 08	0.209632D + 08	− 0.637561D + 08	− 0.249072D + 08	0.209241D + 08	99.91	100.31	100.19
	17	− 0.179760D + 08	− 0.259022D + 08	0.159163D + 07	− 0.178243D + 08	− 0.256925D + 08	0.158829D + 07	100.85	100.82	100.21
	18	− 0.214412D + 07	− 0.102335D + 08	0.127174D + 06	− 0.213039D + 07	− 0.101675D + 08	0.127006D + 06	100.64	100.65	100.13

which are x- and y-directional accelerations at node 43 (load steps 95 and 110), respectively, and the total mass. In Equation (58), 'ne' stands for the number of elements, and d_i^s and d_i^t represent s and t directional cross-sectional dimensions of the ith element, respectively.

The other constraints are

$$c_4 = -\frac{({}^{118}z_1)_{38}}{1.6\times 10^{-1}} - 1.0 \tag{59}$$

$$c_5 = -\frac{({}^{71}\sigma_{11})_{15}}{7.0\times 10^{9}} - 1.0 \tag{60}$$

$$c_6 = -\frac{({}^{74}\sigma_{12})_{15}}{7.0\times 10^{8}} - 1.0 \tag{61}$$

and

$$c_7 = \frac{({}^{118}\varepsilon^{\mathrm{p}}_{\mathrm{eff}})_{15}}{4.5\times 10^{-2}} - 1.0 \tag{62}$$

which are the x-directional displacement at node 38 (at load step 118), the axial stress at element 15 (at load step 71), the shear stress at element 15 (at load step 74), and the plastic strain at element 15 (at load step 118), respectively. The design variable vector $\mathbf{b}$ consists of the cross-sectional dimensions of finite elements in the longitudinal-middle and longitudinal-front components. The initial design and their bounds are

$$b_i = 5.0\times 10^{-2} \tag{63}$$

$$(b_i)_\ell = 10^{-2} \tag{64}$$

and

$$(b_i)_{\mathrm{u}} = 10^{-1} \tag{65}$$

where $i = 1$–48. The results of the optimal design of the vehicle frame are summarized in Table VIII. The constraint violations at the initial design have been removed at the optimum design. The total number of design iterations is 32.

The front longitudinal frame and the first cross component are deformed more at the optimum design, as shown in Figure 8. Note that nodes 38 and 43 deformed less at the optimum design. As a consequence, the total acceleration at node 43 has been reduced greatly as shown in Figure 9. The total acceleration at node 43, which is the cost function, is greatly reduced from 1.00035E + 05 to 9.42576E + 03 as shown in Figure 9.

All constraints at the specified time steps are satisfied. Significant improvements are observed in some of them. In Figure 10, the shear stress at element 15 is generally increased but improved at the specified time step 74. In general, optimization of dynamic problems cannot be carried out to satisfy the constraints for all time steps. This example demonstrates that the desired characteristics can be achieved selectively using the optimization method.

Table VIII. Results for optimum design of vehicle frame.

Cost function	Initial 1.00035E + 05	Optimum 9.42576E + 03
Constraints		
1	1.28253E − 02	− 1.13217E + 00
2	1.48291E − 01	− 7.85414E − 01
3	− 7.50875E − 02	− 5.10425E − 02
4	1.28688E + 00	− 4.78688E − 02
5	3.48466E − 01	− 5.54900E − 01
6	5.29057E − 01	− 6.85186E − 01
7	9.50889E − 01	− 5.62444E − 02

No.	Initial	Optimum	No.	Initial	Optimum	No.	Initial	Optimum
Design variables								
1	5.00000E − 02	1.00000E − 02	2	5.00000E − 02	1.64916E − 02	3	5.00000E − 02	3.15014E − 02
4	5.00000E − 02	2.41634E − 02	5	5.00000E − 02	9.99917E − 02	6	5.00000E − 02	9.99979E − 02
7	5.00000E − 02	1.00000E − 02	8	5.00000E − 02	3.00872E − 02	9	5.00000E − 02	8.29344E − 02
10	5.00000E − 02	9.83872E − 02	11	5.00000E − 02	1.00000E − 02	12	5.00000E − 02	1.00000E − 02
13	5.00000E − 02	1.00000E − 02	14	5.00000E − 02	1.00000E − 02	15	5.00000E − 02	7.06087E − 02
16	5.00000E − 02	3.50284E − 02	17	5.00000E − 02	7.18543E − 02	18	5.00000E − 02	6.46747E − 02
19	5.00000E − 02	1.00000E − 02	20	5.00000E − 02	1.04649E − 02	21	5.00000E − 02	7.65006E − 02
22	5.00000E − 02	6.12811E − 02	23	5.00000E − 02	8.89858E − 02	24	5.00000E − 02	4.22280E − 02
25	5.00000E − 02	5.26490E − 02	26	5.00000E − 02	5.27228E − 02	27	5.00000E − 02	4.94455E − 02
28	5.00000E − 02	4.94302E − 02	29	5.00000E − 02	4.95989E − 02	30	5.00000E − 02	4.95845E − 02
31	5.00000E − 02	5.02055E − 02	32	5.00000E − 02	5.02005E − 02	33	5.00000E − 02	4.99283E − 02
34	5.00000E − 02	4.99652E − 02	35	5.00000E − 02	4.98968E − 02	36	5.00000E − 02	4.99351E − 02
37	5.00000E − 02	4.98873E − 02	38	5.00000E − 02	4.98756E − 02	39	5.00000E − 02	5.11776E − 02
40	5.00000E − 02	5.13509E − 02	41	5.00000E − 02	5.11139E − 02	42	5.00000E − 02	5.15352E − 02
43	5.00000E − 02	5.11101E − 02	44	5.00000E − 02	5.12978E − 02	45	5.00000E − 02	5.03701E − 02
46	5.00000E − 02	5.05415E − 02	47	5.00000E − 02	4.98183E − 02	48	5.00000E − 02	4.98088E − 02

5. CONCLUSION

For crash design optimization, continuum-based sizing design sensitivity analysis (DSA) and optimization methods are developed using DYNA3D for transient dynamic responses of non-linear built-up structures with elastic–plastic material and large deformation. Sizing design sensitivity analysis of kinematic and structural performance measures is carried out. The updated Lagrangian formulation, the explicit time integration, and the direct differentiation method are used for DSA since they are appropriate for highly non-linear path-dependent problems. The Hughes–Liu beam element formulation, and objective stress–strain measures are used for the finite deformation analysis. The elastic–plastic material with combined isotropic/kinematic hardening assumption is employed along with the radial return algorithm. No discontinuous design sensitivity of the stress performance measure is observed at the transition point between the elastic and plastic states due to the radial return method. Numerical implementations of the sizing DSA expressions are performed using DYNA3D. It is recommended to use the fixed time step during the time integration and double precision in the explicit code. The numerical

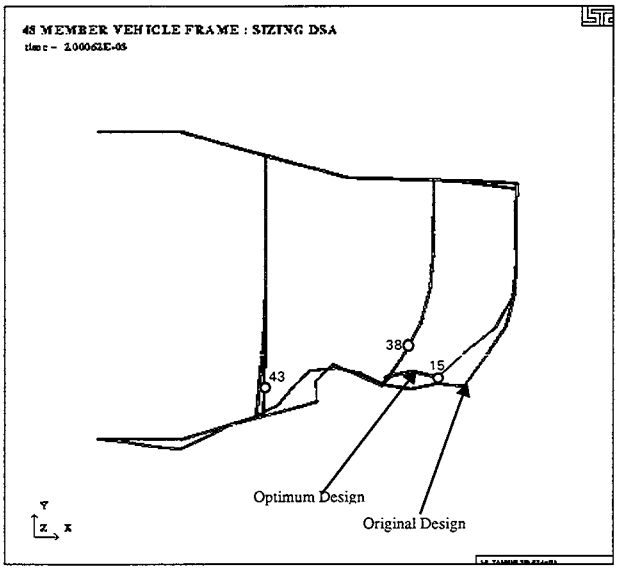

Figure 8. Deformed shapes.

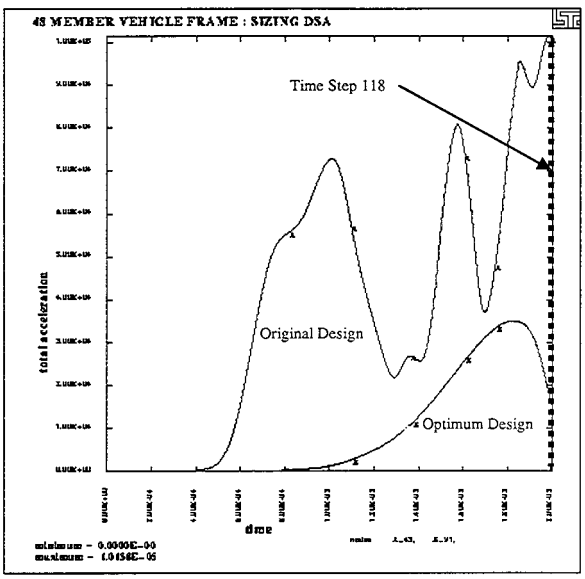

Figure 9. Total acceleration.

examples show that the analytical sensitivity can yield more accurate results than the finite difference results in highly non-linear problems. An iterative design procedure that includes DYNA3D, the developed continuum-based DSA method, and the MFD method shows the applicability of DSA and optimization methods to obtain an optimum design.

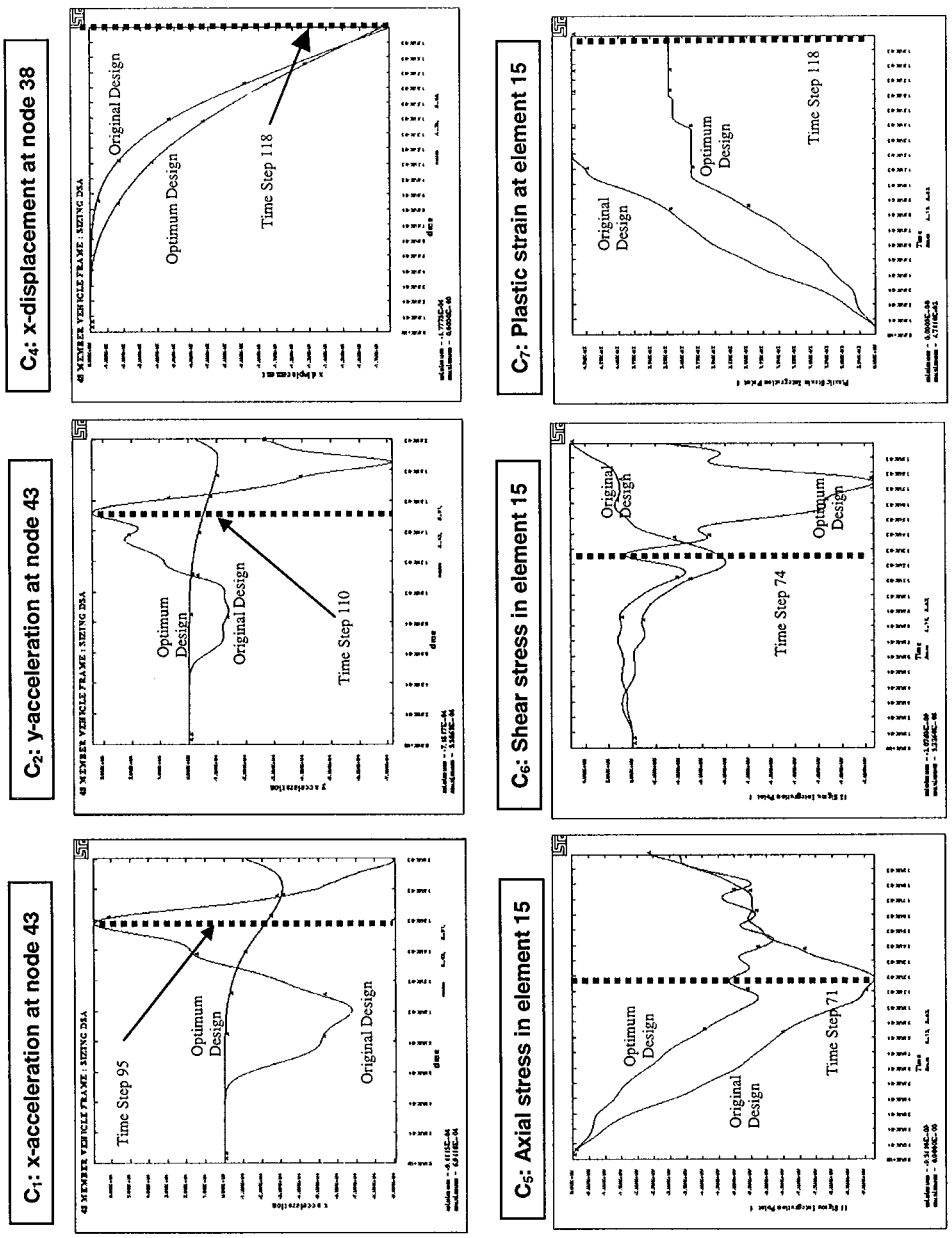

Figure 10. Kinematic and structural response comparison.

APPENDIX: NOMENCLATURE

Unless the configuration number is specified, all the symbols represent the quantities at the current configuration $(n+1)$.

α = back stress tensor
$a(\mathbf{z}, \bar{\mathbf{z}})$ = strain energy form
β = hardening parameter
$\Gamma_d \equiv {}^n\Gamma_d$, $\Gamma_t \equiv {}^n\Gamma_t$ = displacement and traction boundaries at configuration (n), respectively
$\mathbf{C}$ = material response tensor
$\mathbf{d}(t)$ = time-dependent displacement boundary condition
$d(\mathbf{z}_{,tt}, \bar{\mathbf{z}})$ = kinetic energy form
$\dot{\varepsilon}$, $\dot{\varepsilon}^p$, $\Delta\varepsilon$ = strain rate tensor, plastic part of strain rate tensor and increment of strain rate tensor, respectively
ε^p_{eff} = effective plastic strain
E, E_p, E_t, G, K = Young's, plastic, tangent, shear and bulk moduli, respectively
κ = time-step scale factor
$\ell(\bar{\mathbf{z}})$ = load form
ψ = performance measure
ρ = current density
σ, $\dot{\sigma}$, σ^∇, χ = Cauchy stress tensor, material time derivative of Cauchy stress, Jaumann rate of Cauchy stress and deviatoric part of Cauchy stress, respectively
σ_y = yield stress
$T(t)$ = time-dependent traction boundary condition
ω, $\Delta\omega \equiv \mathbf{W}$ = Spin tensor and increment of spin tensor, respectively
$\Omega \equiv {}^n\Omega$ = domain at previous configuration (n)
$\mathbf{X}$, $\mathbf{x}$ = initial and current position vectors, respectively
$\mathbf{x}_I$ = position vector on the reference axis at node I
$\mathbf{x}^+_{\zeta_I}$, $\mathbf{x}^-_{\zeta_I}$, $\mathbf{x}^+_{\eta_I}$, $\mathbf{x}^-_{\eta_I}$ = position vectors located at the top and bottom surfaces, respectively
Y = yield function
$\hat{\mathbf{Y}}_I$, $\hat{\mathbf{Z}}_I$ = unit fibre vectors in y- and z-direction at node I, respectively
$\mathbf{z}$, $\Delta\mathbf{z}$, $\mathbf{z}'$ = displacement, incremental displacement, and first-order variation of displacement vector, respectively
$\mathbf{z}_{,t}$, $\mathbf{z}_{,tt}$ = velocity and acceleration fields, respectively
$\bar{\mathbf{z}}$, Z = virtual displacement and space of kinematically admissible virtual displacement, respectively
$z^+_{\zeta_I}$, $z^-_{\zeta_I}$, $z^+_{\eta_I}$, $z^-_{\eta_I}$ = thickness evaluated at top and bottom surfaces, respectively

ACKNOWLEDGEMENTS

This research is supported by the Automotive Research Center sponsored by the U.S. Army TARDEC. The support is gratefully acknowledged.

REFERENCES

1. Choi KK, Santos JLT. Design sensitivity analysis of nonlinear structural systems. Part I: theory. *International Journal for Numerical Methods in Engineering* 1987; **24**:2039–2055.

2. Santos JLT, Choi KK. Design sensitivity analysis of nonlinear structural systems. Part II: numerical method. *International Journal for Numerical Methods in Engineering* 1988; **26**:2097–2114.
3. Park YH, Choi KK. Design sensitivity analysis of truss structures with elastoplastic material. *Mechanics of Structures and Machines* 1996; **24**(2):189–216.
4. Lee TH, Arora JS. A computational method for design sensitivity analysis of elastoplastic structures. *Computer Methods in Applied Mechanics and Engineering* 1995; **122**:27–50.
5. Tsay JJ, Arora JS. Nonlinear structural design sensitivity analysis for path dependent problems. Part 1: general theory. *Computer Methods in Applied Mechanics and Engineering* 1990; **81**:183–208.
6. Vidal AA, Haber RB. Design sensitivity analysis for rate-independent elastoplasticity. *Computer Methods in Applied Mechanics and Engineering* 1993; **107**:393–431.
7. Hughes TJR, Liu WK. Nonlinear finite element analysis of shells: Part 1. three-dimensional shells. *Computer Methods in Applied Mechanics and Engineering* 1981; **27**:331–362.
8. Hughes TJR, Liu WK. Nonlinear finite element analysis of shells: Part 2. two-dimensional shells. *Computer Methods in Applied Mechanics and Engineering* 1981; **27**:167–181.
9. Hughes TJR, Liu WK, Levit I. Nonlinear dynamics finite element analysis of shells. In *Nonlinear Finite Element Analysis in Structural Mechanics*, Wunderlich E, Stein, Bathe KJ (eds). Springer: Berlin, 1981; 151–168.
10. Hughes TJR, Cohen M, Haroun M. Reduced and selective integration techniques in the finite element analysis of plates. *Nuclear Engineering and Design* 1978; **46**:203–222.
11. Krieg RD, Key SW. Implementation of a time independent plasticity theory into structural computer programs. *Constitutive Equations in Viscoplasticity*: *Computational and Engineering Aspects*, vol. 20. American Society of Mechanical Engineers: New York, NY, 1976; 125–137.
12. Cho S, Choi KK. Design sensitivity analysis and optimization of transient dynamic response of nonlinear structures with elastic–plastic material and large deformation. *Technical Report R99-05*, Center for Computer Aided Design, The University of Iowa, September 1999.
13. Hallquist JO. *Theoretical Manual for DYNA3D*. University of California, Lawrence Livermore National Laboratory, *Report UCID-19401*, 1983.
14. Hughes TJR, Winget J. Finite rotation effects in numerical integration of rate constitutive equations arising in large-deformation analysis. *International Journal for Numerical Methods in Engineering* 1980; **15**:1862–1867.
15. Haug EJ, Choi KK, Komkov V. *Design Sensitivity Analysis of Structural System*. Academic Press: New York, NY, 1986.
16. Hughes TJR, Marsden JE. *Mathematical Foundations of Elasticity*. Prentice-Hall: Englewood Cliffs, NJ, 1983.
17. Simo JC, Taylor R L. Consistent tangent operator for rate-independent elastoplasticity. *Computer Methods in Applied Mechanics and Engineering* 1985; **48**:101–118.
18. Hallquist JO. *LS-DYNA3D Theoretical Manual Rev*. 2, *LSTC Report 1018 Rev*. Vol. 2. 1991.
19. Whirley RG, Engelmann BE. *DYNA3D—A Nonlinear*, *Explicit*, *Three-Dimensional Finite Element Code for Solid and Structural Mechanics User's Manual*, 1993.
20. Malvern LE. *Introduction to the Mechanics of a Continuous Medium*. Prentice-Hall Inc: New Jersey, 1969.
21. Hill R. *The Mathematical Theory of Plasticity*. Oxford University Press: New York, NY, 1971.
22. Lubliner J. *Plasticity Theory*. McGraw-Hill: New York, NY, 1987.
23. Chakrabarty J. *Theory of Plasticity*. McGraw-Hill: New York, NY, 1987.
24. Owen DRJ, Hinton E. *Finite Elements in Plasticity*: *Theory and Practice*. Pineridge Press: Swansea, UK, 1980.

